Inorganic–Organic Composite Cathode Materials for Aqueous Zinc Ion Batteries

Weidong Zhang,[a] Yaokang Lv,*[a] Wei Xiong,[c] Lihua Gan,[b] and Mingxian Liu*[b]

As potential candidates for large-scale energy storage systems, aqueous zinc-ion batteries (AZIBs) have attracted more and more attention from researchers and investors. Tremendous efforts have been devoted to develop high-efficient cathode materials for improving comprehensive performances of AZIBs. Recently reported inorganic-organic composite (IOC) cathode materials exhibited excellent electrochemical performance and were generally superior to corresponding inorganic or organic cathode materials. This paper presents a timely review on recent progresses and challenges in IOCs for AZIBs. Preparation strategies of IOCs have been elaborated and categorized, recent advances and main working mechanisms of IOCs are exhibited with a focus on the analysis methods for mechanism studies, outlooks and challenges of IOC cathodes for AZIBs are outlined to guide their future development.

1. Introduction

Clean renewable energies such as wind and solar energies exhibit instability and intermittency due to environmental limitations.[1–4] Development of cost-effective and environmentally sustainable batteries has become critical in an era marked by rising energy demands and an increasing focus on carbon neutrality.[5–12] As potential candidates for large-scale energy storage systems, aqueous zinc-ion batteries (AZIBs) with high theoretical specific capacity (820 mAh/g) have attracted considerable interest from researchers and investors due to their intrinsic safety, low cost, environmental friendliness as well as mild assembly and testing conditions, compared with commercial lithium-ion batteries and other metal-ion batteries.[13–30]

Cathode materials of AZIBs were considered as the most important factor affecting the performances of AZIBs,[31–34] which can be briefly divided into inorganic cathode materials, organic cathode materials and inorganic-organic composite (IOC) cathode materials.[35–40]

Inorganic cathode materials for AZIBs mainly include manganese oxides, vanadium based compounds and prussian blue analogues. Manganese oxides have layered or channel structures with excellent storage capacity for zinc ions,[41,42] but their chemical instability leads to the continuous dissolution of active substances through Jahn-Teller distortion, resulting in structural collapse and cycling instability.[43,44,69] Compared with manganese oxides, many vanadium based compounds usually

have higher pseudocapacitances and better structural stability,[45–50] but their average operating voltage is relatively low (~0.75 V), which restrict the energy densities of vanadium based compounds.[51–55] Although reported prussian blue analogues have robust frameworks with three-dimensional diffusion channels,[56–59] most of them exhibit poor conductivity and were prone to structural collapse during charge-discharge process.[60,61]

In recent five years, many organic cathode materials for AZIBs have been reported. Organic cathode materials have fascinating features of functional tunability structural diversity as well as resource sustainability.[62–68] Last year, our group firstly reported a new cathode with H-bonded organic superstructures (HBOS) containing cyanuric acid and 1,3,5-triazine-2,4,6-triamine. At a current density of 2 A/g, this HBOS cathode exhibits a capacity of 298 mAh/g.[70] This year, we reported a series of novel self-assembled organic cathode materials featuring with non-metalic NH_4^+/H^+ co-storage, among them benzoquinone-thiourea cathode presents a high discharge capacity of 358 mAh/g at 1 A/g.[71] However, poor conductivity, easy structural damage and deactivation still plague the large scale applications of reported organic cathode materials.

So far, it is difficult for a pristine inorganic or organic cathode material meet the growing demand for energy storage.[71–76] IOC cathode materials were expected to have a synergistic effect by combining suitable inorganic materials with organic materials, the electrochemical performance of reported IOC cathode materials was generally superior to corresponding inorganic or organic cathode materials.[77–80] In this mini-review, we strive to give an overview of IOC cathode materials for AZIBs. Reported IOCs are firstly categorized and summarized with a schematic comparison of their respective preparation strategies and electrochemical properties. The relationships between preparation strategies and structure of IOCs as well as their important electrochemical metrics (working voltages, capacity and cyclic stability) were highlighted for building better AZIBs. Recent advances of IOC cathode materials are exhibited with a focus on their working mechanisms and

[a] W. Zhang, Y. Lv
College of Chemical Engineering, Zhejiang University of Technology, Hangzhou 310014, China
E-mail: yaokanglv@zjut.edu.cn

[b] L. Gan, M. Liu
School of Chemical Science and Engineering, Tongji University, Shanghai 200092, China
E-mail: liumx@tongji.edu.cn

[c] W. Xiong
School of Chemistry and Environmental Engineering, Wuhan Institute of Technology, Wuhan 430205, China

Batteries & Supercaps

Review
doi.org/10.1002/batt.202400507

Chemistry Europe
European Chemical
Societies Publishing

the analysis methods for mechanism studies. Finally, the challenges and outlooks of IOC cathodes and AZIBs are outlined to guide the future development of next-generation energy-related communities.
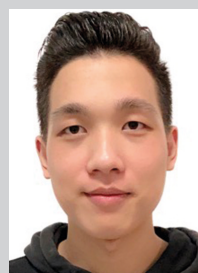
2. IOC Cathode Materials

Researchers have developed a series of high-performance IOC cathode materials for AZIBs in the past decade,[77] while reported IOC cathode materials can be classified into at least two categories, metallic IOCs and carbon based IOCs.

2.1. Metallic IOCs

Many reported metallic IOCs with excellent electrochemical performance were prepared via combining metal compounds with conjugated polymers.[77–90] In 2020, X. Liu et al. prepared ultrathin IOC nanobelts comprising single-crystalline VO_2 and poly (3,4-ethylenedioxythiophene) (PEDOT), which was designated as VO_2-PEDOT. The discharge capacities of VO_2-PEDOT cathode at 0.5 and 8 A/g are 448.5 and 280.2 mAh/g, respectively.[81] Z. Yao et al. reported a V_2O_5@PEDOT cathode material, which is prepared by in-situ polymerization and shallow insertion of 3,4-ethylenedioxythiophene (EDOT) monomer on V_2O_5 (Figure 1). This IOC cathode exhibits excellent cycling performance, after 320 charge-discharge cycles at a current density of 1 A/g, it maintained a capacity of 325 mAh/g.[77] D. Bin et al. employ layered PEDOT-$NH_4V_3O_8$ (PEDOT-NVO) as a cathode material, which exhibits a capacity of 163.6 mAh/g at high current density of 10 A/g, and features an ultra-long lifetime of over 5,000 charge-discharge cycles with a capacity retention of 94.1%.[90] In 2021, X. Liao et al. synthesized a 3D mesoporous microsphere structural IOC material β-MnO_2/PPy, which is composed of β-MnO_2 nanorods and polypyrrole (PPy) nanowires, PPy nanowires compactly linked each individual β-MnO_2 nanorods in series like firecracker. At current density of 0.2 A/g, β-MnO_2/PPy cathode delivered a specific capacity of 361 mAh/g, much higher than that of pure MnO_2.[84] T. Niu et al. coated PPy on α-MnO_2/(reduced graphene oxide, rGO) nanowires via in situ self-polymerization, the obtain IOC material α-MnO_2/rGO-PPy demonstrates reversible capacity of 248.8 mAh/g at 0.5 A/g, which demonstrates enhanced performance compared with α-MnO_2/rGO and α-MnO_2.[86]

In 2022, H. Chen et al. prepared PEDOT-intercalated MnO_2 named PEDOT-MnO_2 through redox precipitation of EDOT, $KMnO_4$ and $MnSO_4$. As shown in Figure 2, the intercalated PEDOT molecules stabilize the crystal structure of MnO_2 and ensure this IOC material with high cycling stability.[82] L. Wang

Weidong Zhang is pursuing his master's degree at Zhejiang University of Technology, where his current research focuses on novel materials as cathode materials for zinc-ion batteries and investigates the reaction mechanism through computational chemistry.

Yaokang Lv received his first Ph. D. degree in Department of Chemistry, Tongji University (2014), and the second Ph. D. degree in Institut de Chimie, Université de Strasbourg (2021). He started his postdoctoral researches in Tsinghua University and joined College of Chemical Engineering at Zhejiang University of Technology as an associate professor in 2020. His current research interests include synthesis and recycling materials for energy storage, electrochromic devices, packaging and pollutants treatment.

Wei Xiong received his PhD degree in Physical Chemistry from Tongji University, China (2012). At present, he works as an Associate Professor in the School of Chemistry and Environmental Engineering at Wuhan Institute of Technology. His main research interests include nanomaterials for energy and environmental applications, such as supercapacitors, electrocatalytic nitrogen reduction, electrochemical sensors and theoretical calculation.
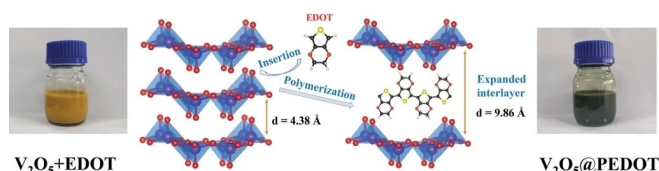
Lihua Gan received his PhD degree from Tongji University, and became a professor at the School of Chemical Science and Engineering in Tongji University (2005). His research interests include the design and application of nanomaterials, which cover porous metal oxides, various carbonaceous materials and carbon-based materials. These nanomaterials are used in supercapacitors, monovalent and multivalent metal ion based batteries and as adsorbents for pollutant treatment.

Mingxian Liu received his Ph.D. degree in physical chemistry in Tongji University (2009). He started his postdoctoral researches in East China University of Science and Technology. After that, he joined School of Chemical Science and Engineering in Tongji University, and became a professor. His current research interests focus on the structural design of electrode materials for electrochemical energy storage including supercapacitors and zinc-ion batteries.

Batteries & Supercaps

Review
doi.org/10.1002/batt.202400507

Chemistry Europe
European Chemical
Societies Publishing

Figure 1. Schematic illustration of V$_2$O$_5$@PEDOT synthesis with photos of solutions at the initial stage (yellow) and final stage (dark green) at room temperature.[77] Copyright (2020) John Wiley and Sons.
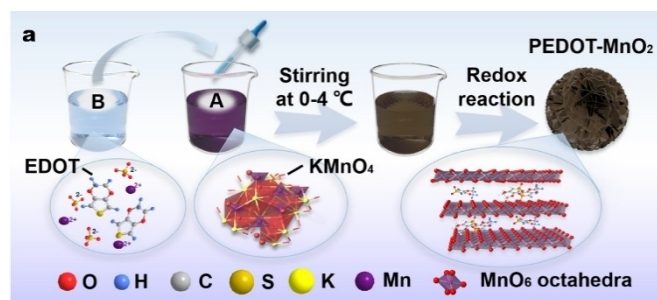

Figure 2. Schematic diagram of the preparation process of PEDOT-MnO2.[82] Copyright (2023) Elsevier.

et al. fabricated PEDOT coated MnO$_2$ (MnO$_2$@PEDOT) using an in situ preparation strategy by mixing EDOT and KMnO$_4$ solution. PEDOT coating improves structural stability and conductivity of MnO$_2$, MnO$_2$@PEDOT cathode reached a capacity of 165.4 mAh/g at 1 A/g.[83]

As shown in Figure 3, K. Cai et al. synthesized porous 3D PPy-coated Mn$_2$O$_3$ microsphere shaped IOC (Mn$_2$O$_3$@PPy) last year, the Mn$_2$O$_3$@PPy cathode presented a reversible specific capacity of 287.7 mAh/g after 300 cycles at 0.1 A/g.[87] This year, B. Sang et al. obtained an IOC of PEDOT intercalated V$_2$O$_5$·nH$_2$O (denoted as PVO-M) using similar synthesize strategy. The presence of PEDOT acts as a "pillar" in PVO-M and leads to an expanded V$_2$O$_5$ interlayer galleries with robust layered structure. As the cathode material for AZIBs, PVO-M delivers a desirable discharge capacity of 513.1 mAh/g at the current density of 0.5 A/g and an excellent cycling stability with 95.3% capacity retention over 2000 cycles.[78] Q. Han et al. coated polypyrrole (PPy) on Mn-ion-substituted zinc hexacyanoferrate (MZHCF) to prepare a IOC cathode material named MZHCF@PPy, which exhibited significant ionic absorption affinity and great structural stability.[101] K. Ran et al. diffused aniline into V$_2$O$_5$ and polymerized in situ to form polyaniline (PANI) chains, an IOC material named PANI80-V$_2$O$_5$, in which was synthesized. In PANI80-V$_2$O$_5$, the V$_2$O$_5$ layer spacing was increased from 5.76 Å to 14.31 Å, thus the diffusion channels and migration pathways
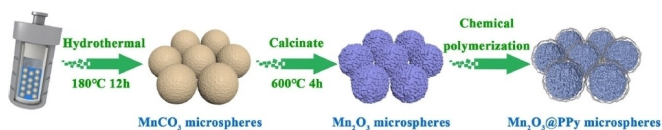
for Zn^{2+} were broadened. At a current density of 0.1 A/g, PANI80-V$_2$O$_5$ cathode exhibited a high discharge capacity of 516.90 mAh/g. At a current density of 10 A/g, it exhibited a discharge capacity of 268.80 mAh/g and a capacity retention rate of 97.77% after 3000 cycles.[80]

Another type of metallic IOCs were obtained through combining metal compounds with small organic molecules.[91–95] In 2021 X. Ma et al reported the solvothermal synthesis of an ethylenediamine (EDA) – vanadium oxide (VO) hybrid IOC material C$_2$H$_8$N$_2$V$_7$O$_{16}$ (denoted as EDA-VO). Benefiting from the structural and compositional features, EDA-VO cathode presents a high capacity (382.6 mAh/g at 0.5 A/g) and extraordinary cycling constancy.[93] In 2022, F. Zhang et al. synthesized the (C$_{12}$H$_{28}$N)$_x$V$_7$O$_{16}$·nH$_2$O nanotubes (denoted as (en)VO) from hydrothermal reaction, then N-(Zn,en)VO with N-doping and oxygen vacancies was further obtained after ion exchanging and NH$_3$ treating (Figure 4). As an IOC cathode material for AZIBs, N-(Zn,en)VO exhibits high capacity of 420.5 mAh/g at 0.05 A/g and long cycle life (4500 cycles without capacity decay at 5 A/g).[91] In 2023, Y. Li et al. reported a IOC material of vanadyl acetate (VO(CH$_3$COO)$_2$, VA) nanostrips which is obtained via solvothermal method. The cathode of VA for AZIBs exhibits high specific capacity (239.0 mAh/g at 500 mA/g) and distinct cycling stability.[94] Y. Tong et al. synthesized methylene blue (MB) intercalated vanadium oxide (denoted as HVO-MB) through sol–gel and ion exchange method. As a cathode material for AZIBs, HVO-MB contributes high rate capability (243 mAh/g at a current density of 5 A/g) and remarkable cycling stability (88% capacity retention after 2000 cycles at 5 A/g).[95]

In general, compared with inorganic cathode materials, metallic IOCs usually have enlarged interlayer spacing and expanded migration channels that alleviate the structural damage caused by Zn^{2+} ions insertion and extraction, promote the diffusion kinetics of Zn^{2+}. The oxygen vacancies and electron mobility of metallic IOCs may also be increased. Thus, as cathode materials for AZIBs, metallic IOCs have the potential to achieve high specific capacity and long cycle stability.
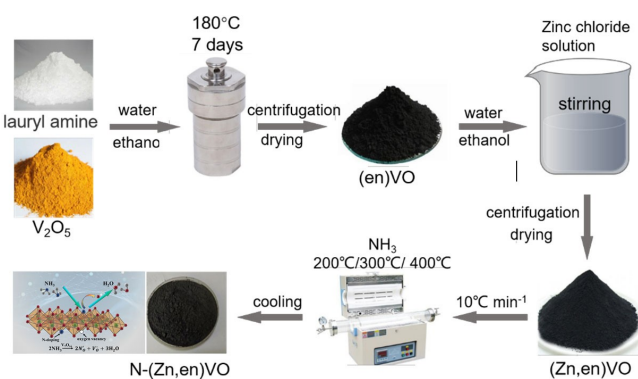

Figure 3. The flow chart of the formation process for mesoporous Mn2O3@PPy.[87] Copyright (2023) Elsevier.

Figure 4. The formation process for mesoporous N-(Zn,en)VO.[91] Copyright (2022) John Wiley and Sons.

2.2. Carbon Based IOCs

Organic cathode with low molecular weight compounds, such as quinones, are often limited by their susceptibility to electrolytic dissolution and low capacity retention.[96] Combining active organic compounds with carbon frameworks is an useful strategy to address the above problems and obtain carbon based IOCs with superior properties.[96–100] In 2020, W. Du et al. discovered that graphene oxide (GO) composited polyaniline (PANI) cathodes show significantly improved zinc-ion storage performance than pure PANI cathodes.[100] In 2021, J. Kumankuma-Sarpong et al. welded small quinones such as naphthoquinone (NQ) onto carbon nanotube (CNT) paper to form IOC cathode films, NQ@CNT. Owing to the high conductivity of CNT networks, NQ@CNT exhibits high rate cyclability.[96] H. Zhang et al. prepared a poly-quinone-phenylenediamine (PONEA)/graphene cathode material through polymerization and hybridization. The AZIBs using this IOC show a specific capacity of 329 mAh/g at 0.1 A/g and significant rate capability with 277 mAh/g at 20 A/g.[97] Y. Zhao et al. proposed two-step electropolymerization method to deposit poly(1,5-naphthalenediamine) and poly(para-aminophenol) in sequence onto nanoporous carbon, designed as C@multi-layer cathode. Benefiting from the synergistic effect, this IOC cathode material presents excellent rate capability (132 mAh/g at 40 A/g) and long lifespan over 5000 cycles.[107] As shown in Figure 5, Y. Zhao et al. electrodeposited poly(meta-aminophenol, 3-AP) and poly((para-aminophenol, 4-AP) layers on the surface of nanoporous carbon to prepare an IOC material, named C@poly(3-AP)/poly(4-AP), which exhibits excellent rate capability of 165 mAh/g at 30 A/g as a cathode material for AZIBs.[109]

In 2022, J. Wang et al. reported a strategy to link electroactive organic building blocks (HATN) using dual thioether bond and then in-situ polymerize it on carbon nanotube (CNT). As shown in Figure 6, the as prepared PAF-205/CNT shows initial capacity of 328.5 mAh/g at 50 mA/g and 89 mAh/g at 20 A/g with 76.2% capacity retention after 10,000 cycles.[98] X. Geng et al. prepared an IOC material of (1,1′-iminodianthraquinone, IDAQ)/rGO as the cathode material for AZIBs, which delivers the capacity of 100 mAh/g at 500 mA/g and 96% capacity retention after 5000 cycles.[99] This year, we proposed an effective anchoring strategy for IOC in which conjugated microporous polymers (CMPs) were successfully anchored onto the suface of rGO via hydrogen bonding and π–π stacking interactions to form rGO@CMPs. Assembled AZIBs based on rGO@CMPs cathode can provide capacities up to 378 mAh/g at 0.2 A/g.[123]
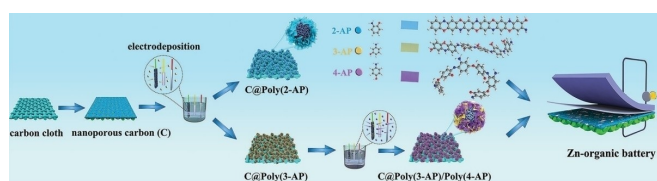

Figure 5. Illustration for the fabrication process of a Zn–organic battery with the C@poly(AP) cathode.[109] Copyright (2021) John Wiley and Sons.
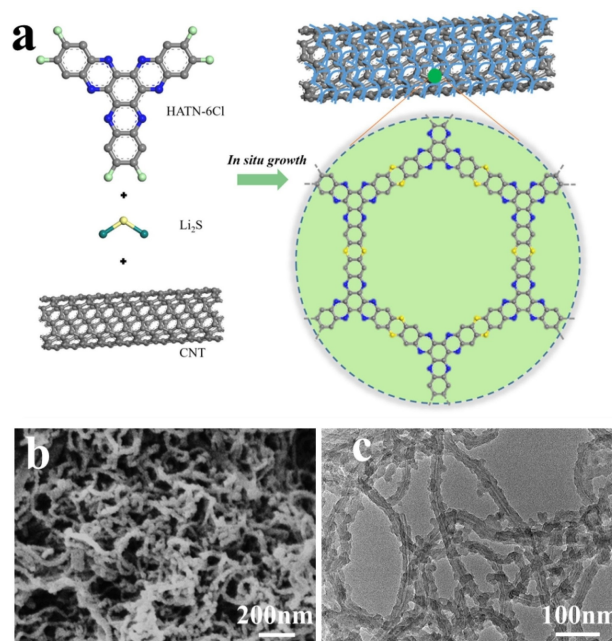

Figure 6. (a) Scheme for the synthetic strategy of PAF-205@CNT. (b) SEM and (c) TEM images of PAF-205@CNT-2.[98] Copyright (2022) Elsevier.

Well-designed carbon based IOCs, which combined the advantages of organic parts and inorganic carbonous parts, can offer large energy densities and long cycle life for AZIBs. Redox-active centers are usually come from organic parts, and carbonous parts can enhance surface area, conductivity and framework stability of IOCs. More advanced carbon based IOCs can be constructed through composite strategies and molecular design.

2.3. Preparation Strategies of IOCs

The preparation strategies and basic electrochemical properties of IOCs reported in the past 5 years are listed in Table 1. So far, intercalation, surface coatings, defective construction and integration are main preparation strategies for IOCs.

2.3.1. Intercalation

Intercalation strategy refers to the formation of a sandwich structure for IOCs in which organic guest molecules are embedded between layers when the inorganic host has a layered structure. Hydrothermal synthesis and in-situ polymerization are common implementation methods for this strategy. Intercalation can provide IOCs with large interlayer spacing and strong structure, thereby enhancing their electrochemical performances for AZIBs. Metallic compounds such as metallic oxides are often used as inorganic hosts due to their rich interlayer configurations, while organic small molecules served as guests are directly embedded and/or in situ polymerized in the hosts' interlayers to form IOCs, such as V_2O_5@PEDOT,[77]

Batteries & Supercaps

Review
doi.org/10.1002/batt.202400507

Chemistry Europe
European Chemical
Societies Publishing

Table 1. Preparation methods and basic electrochemical properties of IOC cathode materials for AZIBs.

IOCs	Preparation strategies	Electrolyte	Working voltage [V]	Specific capacity at x A g^{-1}	Capacity retention at y A g^{-1} after n cycles	Ref.
V_2O_5@PEDOT	Intercalation	3 M Zn(CF$_3$SO$_3$)$_2$	0.2–1.6	452 ($x=1$)	75.8% ($n=4500$, $y=10$)	[77]
PVO-M	Intercalation	3 M Zn(CF$_3$SO$_3$)$_2$ + 0.1 M maltitol	0.2–1.6	513.1 ($x=0.5$)	95.3% ($n=2000$, $y=20$)	[78]
$V_2O_5 \cdot 0.88H_2O$-PANI$_{0.22}$	Intercalation	3 M Zn(CF$_3$SO$_3$)$_2$	0.3–1.6	430 ($x=0.1$)	92% ($n=3000$, $y=5$)	[120]
V_2O_5-Mg-PANI	Intercalation	3 M Zn(CF$_3$SO$_3$)$_2$	0.2–1.6	412 ($x=0.1$)	93% ($n=1000$, $y=2$)	[121]
MVHA	"in-situ substitution" based on MOF-5	1 M ZnSO$_4$	0.3–1.4	312.7 ($x=1$)	82.4% ($n=1000$, $y=10$)	[79]
PANI80-V_2O_5	Intercalation, Defective construction	3 M Zn(CF$_3$SO$_3$)$_2$	0.1–1.6	516.9 ($x=0.1$)	97.8% ($n=1000$, $y=10$)	[80]
VO_2-PEDOT	Intercalation	3 M Zn(CF$_3$SO$_3$)$_2$	0.3–1.3	540 ($x=0.05$)	84.5% ($n=1000$, $y=10$)	[81]
PEDOT-MnO_2	Intercalation	2 M ZnSO$_4$ + 0.2 MnSO$_4$	0.8–1.8	344 ($x=0.2$)	117% ($n=1500$, $y=2$)	[82]
MnO_2@PEDOT	Surface coatings	2 M ZnSO$_4$ + 0.2 MnSO$_4$	1.0–1.8	244 ($x=0.2$)	85% ($n=1000$, $y=2$)	[83]
β-MnO_2/PPy	Integration	2 M ZnSO$_4$ + 0.1 MnSO$_4$	0.8–1.8	362 ($x=0.2$)	96% ($n=160$, $y=0.2$)	[84]
α-MnO_2@2-MI	Surface coatings	2 M ZnSO$_4$ + 0.2 MnSO$_4$	1.0–1.8	399 ($x=0.1$)	68% ($n=2000$, $y=1$)	[85]
α-MnO_2-rGO-PPy	Surface coatings	3 M Zn(CF$_3$SO$_3$)$_2$	0.8–1.8	248.8 ($x=0.5$)	86% ($n=100$, $y=0.5$)	[86]
δ-MnO_2-PEDOT	Surface coatings	2 M ZnSO$_4$ + 0.1 MnSO$_4$	1.0–1.8	243 ($x=0.1$)	99% ($n=100$, $y=0.3$)	[104]
δ-MnO_2-PEDOT-PSS	Surface coatings	2 M ZnSO$_4$ + 0.1 MnSO$_4$	1.0–1.8	219 ($x=0.1$)	99.5% ($n=100$, $y=0.3$)	[104]
Mn_2O_3@PPy	Surface coatings	3 M ZnSO$_4$ + 0.5 M MnSO$_4$	0.8–1.8	353.9 ($x=0.1$)	82.2% ($n=300$, $y=0.1$)	[87]
Mn_3O_4-PPy	Surface coatings	2 M ZnSO$_4$ + 0.2 M MnSO$_4$	0.8–1.9	332.5 ($x=0.1$)	92.5% ($n=1500$, $y=1$)	[88]
α-MoO_3- PEDOT	Intercalation	3 M Zn(CF$_3$SO$_3$)$_2$	0.2–1.4	341.5 ($x=0.1$)	77.6% ($n=500$, $y=30$)	[89]
PANI-MGP-1	Surface coatings	2 M Zn(CF$_3$SO$_3$)$_2$	0.2–1.6	184.5 ($x=0.2$)	72.7% ($n=1000$, $y=2$)	[103]
PEDOT-NVO	Intercalation	3 M Zn(CF$_3$SO$_3$)$_2$	0.4–1.6	356.8 ($x=0.05$)	94.1% ($n=5000$, $y=10$)	[90]
N-(Zn,en)VO	Defective construction	3 M Zn(CF$_3$SO$_3$)$_2$	0.2–1.4	420.5 ($x=0.05$)	100% ($n=4500$, $y=5$)	[91]
TPA-V_{10}	Integration	3 M Zn(CF$_3$SO$_3$)$_2$	0.2–1.8	300 ($x=0.1$)	44% ($n=10000$, $y=10$)	[92]
EDA-VO	Intercalation	3 M Zn(CF$_3$SO$_3$)$_2$	0.4–1.4	382.6 ($x=0.5$)	53% ($n=10000$, $y=5$)	[93]
VO(CH$_3$COO)$_2$	Integration	3 M Zn(CF$_3$SO$_3$)$_2$	0.2–1.7	239 ($x=0.5$)	63% ($n=1000$, $y=5$)	[94]
HVO-MB	Intercalation	3 M Zn(CF$_3$SO$_3$)$_2$	0.3–1.5	418 ($x=0.1$)	88% ($n=2000$, $y=5$)	[95]
PC-G	Integration	3 M ZnSO$_4$	0.2–1.9	355 ($x=0.05$)	74.4% ($n=3000$, $y=1$)	[105]
NQ@CNT	Integration	2 M Zn(CF$_3$SO$_3$)$_2$	0.1–1.65	333.5 ($x=0.339$)	41% ($n=1000$, $y=0.339$)	[96]
Dichlone@CNT	Integration	2 M Zn(CF$_3$SO$_3$)$_2$	0.2–1.8	83.5 ($x=3.39$)	71% ($n=1000$, $y=0.339$)	[96]
APh-NQ@CNT	Integration	2 M Zn(CF$_3$SO$_3$)$_2$	0.1–1.3	160.3 ($x=1.7$)	68.3% ($n=1000$, $y=0.339$)	[96]

Table 1. continued

IOCs	Preparation strategies	Electrolyte	Working voltage [V]	Specific capacity at x A g^{-1}	Capacity retention at y A g^{-1} after n cycles	Ref.
P/G	Integration	3 M Zn(CF$_3$SO$_3$)$_2$	0.2–1.6	329 (x = 0.1)	85 % (n = 4800, y = 10)	[97]
PAF-205/CNT	Integration	2 M Zn(CF$_3$SO$_3$)$_2$	0.3–1.1	328.5 (x = 0.05)	76.2 % (n = 10000, y = 20)	[98]
IDAQ/rGO	Integration	3 M Zn(CF$_3$SO$_3$)$_2$	0.2–1.8	100 (x = 0.5)	96 % (n = 5000, y = 2)	[99]
PAIN-rGO	Integration	2.5 M Zn(CF$_3$SO$_3$)$_2$	0.5–1.6	233 (x = 0.1)	79 % (n = 2500, y = 3)	[100]
PMTP-CNT	Surface coatings	2 M ZnSO$_4$	0.2–1.8	230 (x = 3)	61 % (n = 4000, y = 3)	[106]
C@Pap	Integration	2 M ZnSO$_4$	0.1–18	302 (x = 0.1)	57 % (n = 5000, y = 5)	[107]
C@1,5- NAPD	Integration	2 M ZnSO$_4$	0.1–1.8	275 (x = 0.1)	88 % (n = 5000, y = 5)	[107]
C@multi-layer	Integration	2 M ZnSO$_4$	0.1–1.8	348 (x = 0.1)	83 % (n = 5000, y = 5)	[107]
PDAN-GN	Surface coatings	0.5 M ZnSO$_4$	0.05–1.6	240 (x = 0.1)	100 % (n = 1000, y = 5)	[108]
C@poly(2-AP)	Surface coatings	2 M ZnSO$_4$	0.1–1.8	218 (x = 0.2)	79 % (n = 2000, y = 5)	[109]
C@poly(3-AP)	Surface coatings	2 M ZnSO$_4$	0.1–1.8	235 (x = 0.2)	93 % (n = 2000, y = 5)	[109]
C@poly(4-AP)	Surface coatings	2 M ZnSO$_4$	0.1–1.8	315 (x = 0.2)	85 % (n = 2000, y = 5)	[109]
C@poly(3-AP)/poly(4-AP)	Surface coatings	2 M ZnSO$_4$	0.1–1.8	347 (x = 0.1)	92 % (n = 2000, y = 5)	[109]
p-DB@CF	Integration	3 M Zn(CF$_3$SO$_3$)$_2$	0–1.8	402 (x = 0.1)	93.9 % (n = 25000, y = 5)	[102]
o-DB@CF	Integration	3 M Zn(CF$_3$SO$_3$)$_2$	0–1.8	338 (x = 0.1)	84.9 % (n = 25000, y = 5)	[102]
m-DB@CF	Integration	3 M Zn(CF$_3$SO$_3$)$_2$	0–1.8	302 (x = 0.1)	80.8 % (n = 25000, y = 5)	[102]
MZHCF@PPy	Surface coatings	1 M ZnSO$_4$ + 0.1 M MnSO$_4$	0.8–2.4	190.1 (x = 0.5)	100 % (n = 500, y = 1)	[101]
CoVO@PANI$_{60}$	Surface coatings	3 M Zn(CF$_3$SO$_3$)$_2$	0.2–1.6	456.8 (x = 0.1)	90.4 % (n = 1500, y = 10)	[122]
rGO@CMPs	Integration	2 M Zn(CF$_3$SO$_3$)$_2$	0–1.8	378 (x = 0.2)	90.1 % (n = 25000, y = 10)	[123]
NaNVO@PA	Surface coatings	2 M Zn(CF$_3$SO$_3$)$_2$	0.2–1.6	492 (x = 0.1)	89.2 % (n = 1000, y = 5)	[124]

EDA-VO[93] and α-MoO$_3$- PEDOT.[89] As shown in Table 1, more than ten Metallic IOCs were prepared through intercalation, After intercalation, the interlayer spacing of the inorganic frameworks of these IOCs were obviously increased, and the intercalated organic compounds stabilized the layered structure. Benefiting from this structural features, these IOCs present superior cycling stability.

2.3.2. Surface Coatings

In surface coating strategy, guest organic molecules can be covered onto the surface of the host inorganic materials through adsorption, precipitation, deposition, electrodeposition and in situ polymerization reactions, resulting in various IOCs with different electrochemical properties. Stable conductive network of IOCs can be constructed through introducing appropriate organic coating layer, which facilitates surface electronic and ionic conductivity and enhances the rate capability and cycling performance. For instance, IOCs like α-MnO$_2$-2-MI[85] and PDAN-GN[108] exhibit good conductivity. Recently, X. Liang et al. developed mixed-valence polyoxovanadates [Co$_3$(H$_2$O)$_{12}$][V$^{IV}_{10}$V$^{V}_8$O$_{42}$(SO$_4$)]·24H$_2$O (CoVO) coated by polyaniline (PANI) cathode materials for AZiBs. As shown in Figure 7, density functional theory (DFT) calculations were conducted to further understand the influence of PANI coating on the Zn^{2+} ions storage behavior as well as electronic structure of CoVO. The calculated negative binding energy of 1.769 eV

Batteries & Supercaps

Review
doi.org/10.1002/batt.202400507

Chemistry
Europe
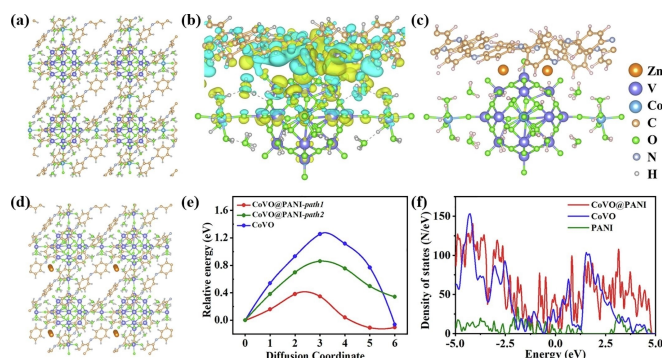European Chemical
Societies Publishing

Figure 7. (a) Theoretical models of CoVO@PANI with Vo. (b) Deformation charge density distribution of the CoVO@PANI (yellow: charge increase; blue: charge decrease) (c) The emptier space between PANI and CoVO host in CoVO@PANI for increasing addition of Zn ions. (d) The migration pathways for Zn2+ in CoVO@PANI. (e) The corresponding energy barriers of Zn2+ diffusion. (f) The corresponding density of states of PANI, CoVO and CoVO@PANI with Vo. Orange, light purple, pale blue, gold, green, blue grey, and gray balls represent Zn, V, Co, C, O, N, and H atoms, respectively.[122] Copyright (2024) Elsevier.

indicates the strong interfacial coupling effects between PANI and CoVO. CoVO@PANI cathode's charge density difference significantly reveals the electronic interaction and charge transfer between different components (Figure 7b). With increasing addition of Zn ions, heterostructure of CoVO@PANI exhibits more emptier space between PANI and CoVO host, the robust contact interfaces in CoVO@PANI enable the excellent electron transfer property and mechanical stability. (Figure 4c) As shown in Figure 4d and e, climbing-image Nudge Elastic Band calculations indicate that the most probable pathway of zinc-ion diffusion is along the interconnected channels formed by $\{V_{18}O_{42}\}$ clusters amd $\{Co(H_2O)_4\}$ bridges with the lowest energy barrier of 0.38 eV. Moreover, total densities of states results show that CoVO@PANI displays a higher density state near the Fermi level, that leads to electrical conductivity enhancement (Figure 7f). These results demonstrates that introducing PANI can provide a complete electron migration path for redox reaction via oxygen vacancies and interfacial optimization, and prevent the dissolution of polyoxovanadate into electrolyte. As a result, CoVO@PANI$_{60}$ cathode with a PANI ratio of 2.3% delivers a high specific capacity of 456.8 mAh/g at the current density of 0.1 A/g, 90.4% of its capacity are retained at 10 A/g for 1500 cycles.[122] M. Ni et al. employed surface coating with polyaniline (PA) to improve the conductivity Na$^+$ and NH^{4+} incorporated V$_2$O$_5$ (NaNVO). As an IOC cathode material for AZIBs, the prepared NaNVO@PA exhibits a remarkable discharge capacity of 492 mAh/g at 0.1 A/g. After 1000 cycles, its capacity retention rate reached 89.2%.[124]

2.3.3. Defective Construction

Introducing suitable amount of defects and vacancies into IOCs can reduce their bandgap, increase the storage sites for zinc ions, promote the diffusion kinetics of H$^+$/Zn^{2+}, and may further improve the reversible specific capacitance of as prepared

AZIBs. K. Ran et al. fabricated an IOC named PANI80-V$_2$O$_5$. The numerous oxygen vacancies of PANI80-V$_2$O$_5$ increased the storage sites of Zn^{2+} ions, mitigated the strain on the material structure caused by Zn^{2+} ions intercalation-deintercalation, and promoted the Zn^{2+} ion diffusion kinetics.[80]

2.3.4. Integration

Integration strategy is combining active organic compounds with inorganic materials utilizing chemical bonds and intermolecular interactions to prepare IOCs. Integration strategy is one of the most popular strategies, more than 18 recently report IOCs were prepared via integration processing (Table 1). For example, X. Dan et al. combined V$_{10}$O$_{28}$$^{6-}$ clusters (V10) with protonated 4-amino-p-terphenyl (TPA) in a methanol/water solution and built a polyoxovanadate-based hydrophobic 2D layered IOC (TPA-V10). TPA-V10 delievers a higher operating voltage (0.94 V) and specific capacity (300 mAh/g after 100 cycles at 0.1 A/g), as well as an extended cycle life (surpassing 10000 cycles at 10 A/g) compared to those of V10.[92] H. Zhang et al. combined poly-quinone-phenylenediamine with graphene and obtained an IOC named P/G in order to improve the electrical conductivity of cathode materials. In P/G, polymer and graphene tight coupled and formed reticulate structure under π-π interactions. The Zn//P/G batteries can deliver a specific energy density of 242 Wh/kg at a power density of 71 W/kg.[97]

2.3.5. Other Preparation Strategy

Last year, Z. Luo et al. proposed an "in-situ substitution strategy" to synthesize IOCs by using metal organic frameworks (MOFs) such as MOF-5 (C$_{24}$H$_{12}$O$_{13}$Zn$_4$) as the matrix. After a hydrothermal treatment, in-situ substitution between V and Zn took place, and a new compound MOF-5-V was formed. Attributing to the particular organistructure, MOF-5-V could act as a physical barrier to inhibit the cathodic dissolution. As depicted in Figure 8, the as prepared IOC cathode material (named MVHA) contained MOF-5-V, VO$_2$ and Zn$_2$V$_2$O$_7$. MVHA cathode could deliver a high specific capacity (312.7 mAh/g at 1 A/g), and good cycle stability.[79] Introducing MOFs into IOCs
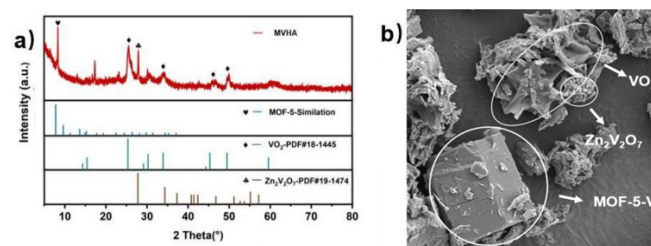

Figure 8. (a) XRD patterns of MVHA and the standard patterns of MOF-5, VO2·xH2O (PDF#18-1445) and ZnV2O7 (PDF#19-1474); (b) Detailed distribution of each component in MVHA.[79] Copyright (2023) Elsevier.

Batteries & Supercaps

Review
doi.org/10.1002/batt.202400507

Chemistry
Europe

European Chemical
Societies Publishing

Table 2. Working mechanisms and analysis methods of IOC cathode materials for AZIBs.

IOCs	Working mechanisms	Analysis methods	Ref.
PVO-M	co-insertion mechanism (Zn^{2+}/H^+)	XRD/XPS/EDS	[78]
MVHA	co-insertion mechanism (Zn^{2+}/H^+)	XRD/XPS/EDS/SEM	[79]
PANI80-V_2O_5	Zn^{2+} insertion/deinsertion mechanism	XRD/XPS/RS	[80]
VO_2-PEDOT	co-insertion mechanism (Zn^{2+}/OTF^-)	XRD/XPS/RS	[81]
PEDOT-MnO_2	chemical transformation reaction mechanism	XRD/XPS/SEM	[82]
α-MnO_2@2-MI	chemical transformation reaction mechanism	XRD/XPS/EDS	[85]
Mn_2O_3@PPy	chemical transformation reaction mechanism	XRD/XPS/SEM	[87]
α-MoO_3- PEDOT	Zn^{2+} insertion/deinsertion mechanism	XRD/XPS	[89]
PEDOT-NVO	Zn^{2+} insertion/deinsertion mechanism	XRD/XPS	[90]
TPA-V_{10}	Zn^{2+} insertion/deinsertion mechanism	XRD/XPS	[92]
EDA-VO	Zn^{2+} insertion/deinsertion mechanism	XRD/XPS/HRTEM	[93]
HVO-MB	co-insertion mechanism ($Zn^{2+}/H^+/CF3SO_3^-$)	XRD/XPS/RS	[95]
PONEA/rGO	co-insertion mechanism ($Zn^{2+}/CF3SO_3^-$)	XPS/EDS	[97]
PAF-205/CNT	co-insertion mechanism (Zn^{2+}/H^+)	EPR/XRD/XPS/CV/RS	[98]
IDAQ/rGO	co-insertion mechanism (Zn^{2+}/H^+)	CV	[99]
PMTP-CNT	Zn^{2+} insertion/deinsertion mechanism	XRD/XPS/RS/SEM	[106]
C@multi-layer	Zn^{2+} insertion/deinsertion mechanism	XPS/RS	[107]
PDAN-GN	Zn^{2+} insertion/deinsertion mechanism	XRD	[108]
p-DB@CF	co-insertion mechanism (Zn^{2+}/OTF^-)	FT-IR/RS/XPS	[102]

through this strategy may obtain ideal cathodes with high complexity for AZIBs.

3. Working Mechanism Studies and Analysis Methods for IOCs

Studying the working mechanism of IOCs during charging-discharging process, identifying the intrinsic relationships between the performances and structure of IOC cathodes, as well as the key bottlenecks limiting their application, are very important for corresponding AZIBs design and the further improvement of their energy and power density.[110–124] In our previous review, the working mechanism of AZIBs' cathode materials was roughly divided into five categories, they are Zn^{2+} insertion/deinsertion mechanism, chemical conversion reaction mechanism, co-insertion mechanism, combined intercalation conversion reaction and dissolution-deposition reaction mechanism. The working mechanism studies through theoretical calculations were also discussed.[110] Nevertheless, adequate experimental analysis data is important and necessary to gain deep insights into the electrochemical process of IOCs and validate theoretical calculation results. As listed in Table 2, recently reported working mechanisms regarding IOC cathode materials mainly include Zn^{2+} insertion/deinsertion mechanism, co-insertion mechanism and chemical transformation reaction mechanism, and analysis methods that support these mechanism studies include: cyclic voltammetry (CV), X-Ray diffraction (XRD), X-ray photoelectron spectroscopy (XPS), high-resolution transmission electron microscopy (HRTEM), scanning electron microscopy (SEM) and Energy dispersive spectroscopy (EDS), Fourier transform infrared spectroscopy (FT-IR), Raman spectroscopy (RS), ex-situ electron paramagnetic resonance (EPR) measurement and son on.[78–102]

3.1. CV Analysis

CV is an electrochemical analysis technique that studies the kinetics and mechanism of electrochemical reactions by applying a linearly varying potential (voltage) on the electrode surface and monitoring the corresponding current response. Through CV, It is easy to directly observe and quickly understand the redox reactions on the electrode, as well as the reversibility of reactions.[97,98] Therefore, working mechanism and kinetic analyses of IOCs can be investigated by CV tests. As shown in Figure 9a, two pairs of redox peaks were appeared in the CV curves of p-DB@CF at scan rates of 1–10 mV/s, revealing the existence of two consecutive charge storage steps on the p-DB@CF cathode.[102] As depicted in Figure 9b, a pair of main peak at 0.53/0.33 V are existed in both CV curves of IDAQ and IDAQ/rGO cathodes, verifying the insertion/deinsertion of Zn^{2+} at the carbonyl center, Besides, the peak at 0.88/0.79 V was resulted from the weeny interaction of imino with zinc ions, while the peak at 0.63/0.57 V was caused by the tiny interaction of hydroxyl with zinc ions.[99] As shown in Figure 9c, CV curves of PANI80-V_2O_5 cathode exhibited an identical shape with the increase in the scan rate, indicating a high tolerance to Zn^{2+} insertion/deinsertion.[80] As shown in Figure 9d, there are two cathodic peaks appear at 1.22 V and 1.39 V and the corresponding anodic peak appears at around 1.59 V with a shoulder at
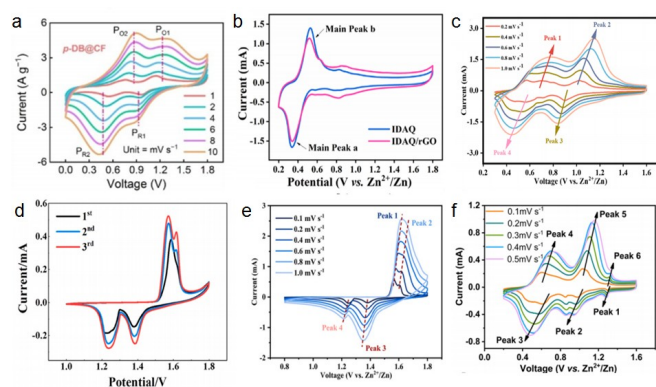
Figure 9. CV curves of (a) p-DB@CF cathode at scan rates of 1–10 mV/s;[102] Copyright (2022) John Wiley and Sons. (b) cathodes of IDAQ and IDAQ/rGO;[99] Copyright (2022) American Chemical Society. (c) PANI80-V2O5 cathode at a sweep rate range of 0.2–1.0 mV/s;[80] Copyright (2024) Elsevier. (d) α-MnO2@2-MI cathode at scan rate of 0.1 mV/s;[85] Copyright (2022) Elsevier. (e) Mn2O3@PPy cathode;[87] Copyright (2023) Elsevier. (f) PVO-M cathode at scanning rates of 0.1–0.5 mV/s.[78] Copyright (2024) Elsevier.

1.60 V in the first CV cycle of α-MnO$_2$@2-MI, but the anodic peak slightly shifts toward lower potentials (around 1.57 V) and the shoulder peak moves to 1.62 V in the second and third cycles. This phenomenon indicates that α-MnO$_2$@2-MI may undergo structural change after cycling.[85] Figure 9e presents the CV curves of Mn$_2$O$_3$@PPy cathode at scan rates of 0.1–1 mV/s. In the CV curve at slow (0.1 mV/s) scan rate, the insertion peak 3 of H$^+$ firstly emerged first, followed by the insertion peak 4 of Zn^{2+}. Upon increasing scanning speed, the intensity of peak 3 increased gradually relative to that of peak 4, which suggests that H+-ion intercalation should be the predominant reaction at high current densities.[87] As presented in Figure 9f, three pairs of redox peaks can be observed in the CV curves of PVO-M cathode.The shape of redox peaks maintain similar with scan rates increasing.[78]

Furthermore, engery storage process of AZIBs can be further divided into capacitive and ionic diffusion contributions, which also could be estimated through data of CV.[97]

Practically, relationship between scan rates (v) and peak currents (I) of CV usually can be explained as below:

$$I = av^b \tag{1}$$

In this Equation (1), parameters "a" and "b" are adjustable, The values of "b" between 0.5 to 1 and can be calculated by the slope from the log(I) versus log(v) plots. If "b" equals 0.5, the charge/discharge process is considered to be completely ionic diffusion-controlled, but if "b" is equal to 1.0, it is regarded as a complete capacitor-like process.

Equation (1) can be also reformulated as follow:

$$I = k_1 v + k_2 v^{1/2} \tag{2}$$

where the values of "k_1" and "k_2" are the capacitive contribution part and the ionic diffusion contribution part, respectively.

For example, based on the CV data of PVO-M cathode,[78] at the scan rate of 0.1 mV/s, the capacitive contribution were calculated to be 40% of the total capacity, as the scan rate increases to 0.5 mV/s, capacitive contribution rises to 66% gradually.

3.2. XRD Analysis

Ex-situ and/or in-situ XRD analyses are useful to observe the changes in crystalline phase of IOC cathodes during charge-discharge process at the selected states.

As depicted in Figure 10, ex-situ XRD patterns of Mn$_2$O$_3$@PPy during charging-discharging revealed that the original diffraction peaks of Mn$_2$O$_3$@PPy had not shift during charging-discharging, indicating that the lattice distortion caused by Zn^{2+} ions intercalation/deintercalation was very tiny.[87] Several new diffraction peaks attributed to the formation of layered Zn$_4$SO$_4$(OH)$_6\cdot$5H$_2$O (ZHS, JCPDS card 39–0688) emerged in the XRD patterns during charging process, indicating that ZHS was produced through the reactions of inserted Zn^{2+} with OH$^-$, SO$_4^{2-}$ and H$_2$O. A reversible diffraction peak at approximately 17° during cycling corresponded to the Zn$_x$Mn$_2$O$_3$ phase, which indicated that Zn^{2+} ions insertion was involved in discharging process. Besides, diffraction peaks at approximately 26°, 58°, and 59° are corresponded to MnO (JCPDS card 04-0326), which confirmed the insertion of H$^+$ ions into the cathode material. These results demonstrate that the working mechanism of Mn$_2$O$_3$@PPy involved Zn^{2+} and H$^+$ co-insertion.

As shown in Figure 11, to elucidate the working mechanism of of EDA-VO, in-situ XRD was performed to investigate the structural evolutions during galvanostatic charge-discharge cycles. Upon discharge, the (002) peak of EDA-VO shifts from 10° to 9.5°, which reveals the lattice expansion at the intercalation of Zn^{2+} into the parallel tunnels. This peak shifts reversibly to the original location and retains cyclical fluctuation in the next cycle, indicating good reversibility of Zn^{2+} insertion/deinsertion in EDA-VO.[93]
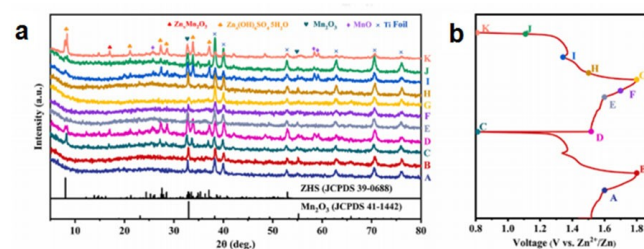

Figure 10. (a) Ex-situ XRD patterns and (b) the corresponding constant current charge-discharge curve of the Mn2O3@PPy cathode.[87] Copyright (2023) Elsevier.

Batteries & Supercaps

Review
doi.org/10.1002/batt.202400507

Chemistry Europe
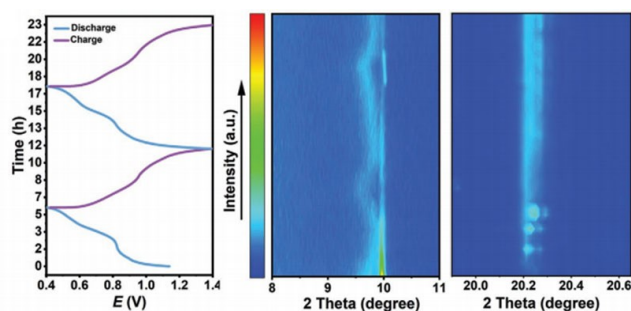European Chemical
Societies Publishing

Figure 11. Left: the corresponding discharge/charge profiles of the Zn/EDA-VO in-situ XRD battery. Right: 2D contour plots of the in-situ XRD patterns showing the 2θ region during two complete charge-discharge cycles.[93] Copyright (2022) John Wiley and Sons.

3.3. XPS Analysis

Ex-situ XPS can be applied to observe transformation of elemental valence states in IOC cathodes during charge-discharge cycles. Figure 12a shows the ex-situ XPS results of V 2p in MVHA at different states, peak ratios of V^{5+}, V^{4+} and V^{3+} are 0.16, 0.56, and 0.28 at the original state, respectively. In full discharge state, because of the insertion of Zn^{2+}, the ratios become 0.19, 0.44, and 0.37, demonstrating the reduction of the V element. With the deinsertion of the Zn^{2+} until full charge state, V^{3+} peak has been disappeared, only V^{5+} and V^{4+} peaks remain in XPS curves. XPS curves of Zn 2p are shown in Figure 12b, the strong peaks at 1045.4 eV and 1022.4 eV correspond to $2p^{1/2}$ and $2p^{3/2}$ of Zn element in MVHA. The intensity of the peaks is high in the full discharge state while low in the full charge state, illustrating the insertion/extraction of Zn^{2+}. XPS curves of O 1s are shown in Figure 12c, during discharge process, the content of water molecules increases gradually, while the content of V—O bond decreases continuously, which proves that H^+ continues to embed and VO_2 is converted to $Zn_4(OH)_6SO_4 \cdot 5H_2O$.[79]
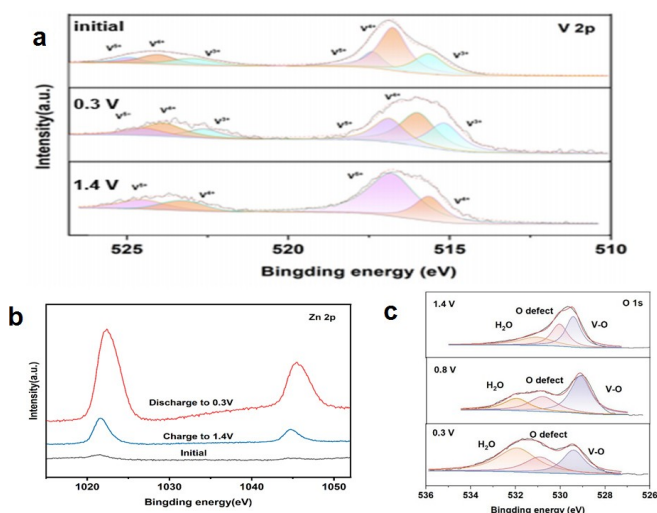

Figure 12. Ex-situ XPS spectra of (a) V 2p, (b) Zn 2p, (c) O 1s in the second cycle at different states.[79] Copyright (2023) Elsevier.

3.4. HRTEM, SEM and EDS Analyses

Ex-situ HRTEM analysis of EDA-VO provides evidences for their working mechanism. As shown in Figure 13, the (300) plane of pristine EDA-VO exhibits lattice fringe with d-spacing of 0.21 nm (Figure 13a). When EDA-VO was discharged to 0.4 V, the corresponding interplanar spacing was extended to 0.237 nm (Figure 13b). When EDA-VO was charged to 1.4 V, the interplanar spacing was narrowed into 0.211 nm, almost totally recovered into initial state (Figure 13c). These results prove good reversibility of Zn^{2+} insertion/deinsertion in EDA-VO.[93]

The morphology evolution for IOC cathode can also be observed by SEM to explore electrochemical reactions occurring at the cathode surface. As shown in Figure 14, the SEM analysis results reveal the highly reversible morphological evolution of the surface of PEDOT-MnO₂-2 cathode during charging-discharging process. When the AZIB was fully discharged to 0.8 V, a large number of micron-sized ZSH flakes can be observed on the surface of cathode (Figure 14b), and when the AZIB was fully charged to 1.8 V, most of these ZSH flakes are disappeared (Figure 14c).[82]

SEM-EDS mapping images of IOCs at fully charged and disharged state can also provide evidences for their working mechanism. As shown in Figure 15a, when PONEA/rGO cathode was fully discharged to 0.2 V, an obvious signal of the Zn element can be recognized, sugggesting the insertion of Zn^{2+}
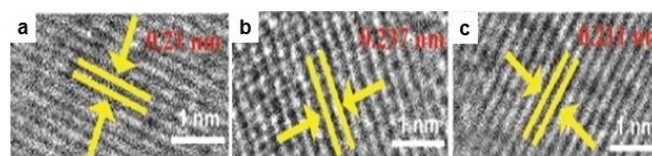

Figure 13. HRTEM images of EDA-VO cathodes at a) initial, b) fully discharged, and c) fully charged states.[93] Copyright (2022) John Wiley and Sons.
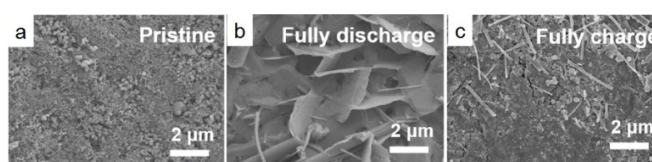

Figure 14. SEM images of (a) pristine, (b) fully discharge, and (c) fully charge states of PEDOT-MnO2-2 cathode.[82] Copyright (2023) Elsevier.
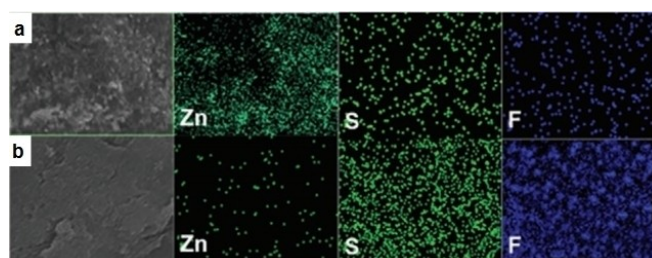

Figure 15. SEM images and SEM-EDS mapping of Zn, S, F elemental distributions on PONEA/rGO cathode at (a) fully discharged (0.2 V), and (b) fully recharged (1.6 V) states.[97] Copyright (2021) John Wiley and Sons.

into the cathode. As shown in Figure 15b, when PONEA/rGO was fully recharged to 1.6 V, the signal of Zn element was significantly weakened but the signals of S and F elements were enhanced, indicating the binding of $CF_3SO_3^-$ in the aqueous electrolyte. These results suggest that PONEA/rGO cathode manifest a hybrid mechanism involving the insertion/extraction of Zn^{2+} and the binding/removal of $CF_3SO_3^-$.[97]

3.5. Other Analyses

Several characteristic peak intensities of RS were increased or decreased during charging-discharging process, it have been reported that in-situ or ex-situ RS analyses were conducted to study the working mechanism of IOCs.[80,102] The detailed working mechanism of IOC cathodes could also be inferred by ex-situ FT-IR spectra which can capture the changes in the intensity and position of characteristic absorption peaks corresponding to organic functional groups of IOCs in different redox states.[106] Besides, if single electron substances such as radicals are involved in the redox reactions of the IOC cathodes, ex-situ EPR measurement at different states of IOCs can be used to reveal their mechanisms.[98]

4. Summary and Outlook

By introducing and collating the development IOC cathode materials for AZIBs in recent years, it has been found that the preparation strategy largely determines the structure and electrochemical performance of IOCs, while working mechanism studies IOCs are important for targeted design of IOCs structure to further improve their comprehensive performance. We elaborated and categorized the preparation strategies of IOCs, and exhibited recent advances and main working mechanisms of IOCs with a focus on the analysis methods for mechanism studies. Some suggestions for preparing better IOCs and AZIBs were proposed herein.

I. Compared with metal oxides, polyoxometalates (POMs) exhibit high chemical tunability and various active sites for redox reactions. So far, only a few researches focused on the application of POMs in AZIBs due to the solubility of POMs in aqueous solutions.[92,122] Devloping novel preparation strategies for IOCs based on POMs would be a promising research direction.

II. In order to prepare AZIB with excellent performance, it is necessary to select compatible electrode materials and electrolytes. So far, only a few researches focus on the interaction between IOC cathode materials and different electrolytes.

III. Several in-situ and ex-situ analysis methods have been used to provide experimental data support working mechanism studies of IOCs. Considering the limitations of the observation range of electron microscopy, and the difficulty to ensure the same observation position of the samples in ex-situ analyses, in-situ SEM and in-situ TEM are recommended to obtain more reliable data. More advanced analysis

methods such as in situ solid-state nuclear magnetic resonance analysis and differential electrochemical mass spectrometry are suggested for mechanism studies.

Conflict of Interests

The authors declare no conflict of interest.

[1] L. Wang, X. Cao, L. Xu, J. Chen, J. Zheng, *ACS Sustainable Chem. Eng.* **2018**, *6*, 16055–16063.
[2] S. Luo, J. Xu, B. Yuan, L. Xu, R. Zheng, Y. Wang, M. Zhang, Y. Lu, Y. Luo, *Carbon* **2023**, *203*, 326–336.
[3] X. Wu, C. Yin, M. Zhang, Y. Xie, J. Hu, R. Long, X. Wu, X. Wu, *Chem. Eng. J.* **2023**, *452*, 139573.
[4] B. Fei, Z. Liu, J. Fu, X. Guo, K. Li, C. Zhang, X. Yang, D. Cai, J. Liu, H. Zhan, *Adv. Funct. Mater.* **2023**, *33*, 2215170.
[5] Y. Qin, S. Jha, C. Hu, Z. Song, L. Miao, Y. Chen, P. Liu, Y. Lv, L. Gan, M. Liu, *J. Colloid Interface Sci.* **2024**, *675*, 1091–1099.
[6] W. Zhang, T. Wang, X. Xing, H. Yin, J. Li, W. Xiong, H. Li, *ACS Sustainable Chem. Eng.* **2024**, *12*, 10313–10324.
[7] W. Xiong, H. Yin, X. Xing, H. Li, *J. Chem. Educ.* **2024**, *101*, 1233–1240.
[8] S. Wu, X. Xing, W. Xiong, Z. Guo, H. Li, *Sensors Actuat. B- Chem.* **2024**, *413*, 135908.
[9] X. Huang, X. Xing, W. Xiong, H. Li, *Carbon Lett.* **2024**, *34*, 1197–1206.
[10] J. Li, H. Yu, Y. Lv, Z. Cai, Y. Shen, L. Ruhlmann, L. Gan, M. Liu, *Nanotechnology* **2024**, *35*, 152001.
[11] Y. Lv, J. Wang, D. Ji, J. Li, S. Zhao, Y. Zhao, Z. Cai, X. He, X. Sun, *Front. Energy Res.* **2023**, *10*, 957032.
[12] Y. Lv, L. Huang, C. Chen, Z. Cai, L. Ruhlmann, *ChemistrySelect* **2024**, *9*, e202401225.
[13] Z. Wang, M. Zhang, W. Ma, J. Zhu, W. Song, *Small* **2021**, *17*, 2100219.
[14] Z. Li, T. Beyene, K. Zhu, D. Cao, *J. Met. Mater. Miner.* **2024**, *34(2)*, 2009.
[15] W. Sun, F. Wang, S. Hou, C. Yang, X. Fan, Z. Ma, T. Gao, F. Han, R. Hu, M. Zhu, C. Wang, *J. Am. Chem. Soc.* **2017**, *139*, 9775–9778.
[16] X. Gao, W. Yin, X. Liu, *Mater. Res. Bull.* **2021**, *138*, 111246.
[17] J. Song, W. Wang, Y. Fang, S. Wang, D. He, R. Zhao, W. Xue, *Appl. Surf. Sci.* **2022**, *578*, 152053.
[18] B. Wu, G. Zhang, M. Yan, T. Xiong, P. He, L. He, X. Xu, L. Mai, *Small* **2018**, *14*, 1703850.
[19] M. Wang, Y. Cheng, H. Zhao, J. Gao, J. Li, Y. Wang, J. Qiu, H. Zhang, X. Chen, Y. Wei, *Small* **2023**, *19*, 2302105.
[20] S. Kim, J. Kim, D. Ahn, S. Lee, *Small* **2020**, *16*, 2002837.
[21] O. Buyukcakir, R. Yuksel, F. Begar, M. Erdogmus, M. Arsakay, S. Lee, S. Kim, R. Ruof, *ACS Appl. Energ. Mater.* **2023**, *6*, 7672–7680.
[22] Q. Sun, T. Sun, J. Du, C. Xie, D. Yang, G. Huang, H. Xie, X. Zhang, *Angew. Chem. Int. Ed.* **2023**, *62*, e202307365.
[23] Z. Gong, Z. Li, P. Wang, K. Jiang, Z. Bai, K. Zhu, J. Yan, K. Ye, G. Wang, D. Cao, G. Chen, *Adv. Energy Mater.* **2023**, *4*, 0035.

[24] Q. Zhao, W. Huang, Z. Luo, L. Liu, Y. Lu, Y. Li, L. Li, J. Hu, H. Ma, J. Chen, *Sci. Adv.* **2018**, *4*, eaao1761.

[25] F. Ye, Q. Liu, H. Dong, K. Guan, Z. Chen, N. Ju, L. Hu, *Angew. Chem. Int. Ed.* **2022**, *61*, e202214244.

[26] S. Xie, X. Li, Y. Li, Q. Liang, L. Dong, *Chem. Rec.* **2022**, *22*, e202200201.

[27] Z. Lin, H. Shi, L. Lin, X. Yang, W. Wu, X. Sun, *Nat. Commun.* **2021**, *12*, 4424.

[28] F. Ye, Q. Liu, H. Dong, K. Guan, Z. Chen, N. Ju, L. Hu, *Angew. Chem. Int. Ed.* **2022**, *61*, e202214244.

[29] J. Chen, H. Chang, Z. Liu, Z. Chen, S. Han, X. Cao, S. Liang, *J. Power Sources* **2024**, *613*, 234904.

[30] H. Cui, L. Ma, Z. Huang, Z. Chen, C. Zhi, *SmartMat* **2022**, *3*, 565–581.

[31] Y. Zeng, X. Zhang, R. Qin, X. Liu, P. Fang, D. Zheng, Y. Tong, X. Lu, *Adv. Mater.* **2019**, *31*, 1903675.

[32] S. Hwang, S. Seo, D. Kim, *J. Mater. Chem A.* **2022**, *10*, 10638.

[33] J. Zhang, W. Li, J. Wang, X. Pu, G. Zhang, S. Wang, N. Wang, X. Li, *Angew. Chem. Int. Ed.* **2023**, *62*, e202215654.

[34] M. Chamoun, W. Brant, C. Tai, G. Karlsson, D. Noréus, *Energy Storage Mater.* **2018**, *15*, 351–360.

[35] C. Wei, C. Xu, B. Li, H. Du, F. Kang, *J. Phys. Chem. Solids* **2012**, *73*, 1487–1491.

[36] J. Lee, J. Ju, W. Cho, B. Cho, S. Oh, *Electrochim. Acta* **2013**, *112*, 138–143.

[37] L. Zhang, L. Chen, X. Zhou, Z. Liu, *Adv. Energy Mater.* **2015**, *5*, 1400930.

[38] S. Lee, G. Nam, J. Sun, J. Lee, H. Lee, W. Chen, J. Cho, Y. Cui, *Angew. Chem. Int. Ed.* **2016**, *55*, 8599–8604.

[39] J. Jo, Y. Sun, S. Myung, *J. Mater. Chem. A* **2017**, *5*, 8367–8375.

[40] H. Ma, X. Tian, T. Wang, K. Tang, Z. Liu, S. Hou, H. Jin, G. Cao, *Small* **2021**, *17*, 2100746.

[41] C. Yuan, Y. Zhang, Y. Pan, X. Liu, G. Wang, D. Cao, *Electrochim. Acta* **2014**, *116*, 404–412.

[42] Z. Tang, Z. Wen, Z. Lyu, Q. Chen, *Adv. Energy Mater.* **2022**, *2022*, 9765710.

[43] M. Song, H. Tan, D. L. Chao, H. J. Fan, *Adv. Funct. Mater.* **2018**, *28*, 1802564.

[44] X. Guo, J. Zhou, C. L. Bai, X. K. Li, G. Z. Fang, S. Q. Liang, *Mater. Today Energy* **2020**, *16*, 100396.

[45] W. Zhang, C. Tang, B. Lan, L. Chen, W. Tang, C. Zuo, S. Dong, Q. An, P. Luo, *J. Alloys Compd.* **2020**, *819*, 152971.

[46] G. Qu, K. Guo, W. Chen, Y. Du, Y. Wang, B. Tian, J. Zhang, *Energy Environ. Mater.* **2023**, *6*, e12502.

[47] N. Qiu, Z. Yang, R. Xue, Y. Wang, Y. Zhu, W. Liu, *N. Lett.* **2021**, *21*, 2738–2744.

[48] W. Liu, L. Dong, B. Jiang, Y. Huang, X. Wang, C. Xu, Z. Kang, J. Mou, F. Kang, *Electrochim. Acta* **2019**, *320*, 134565.

[49] P. Luo, W. Zhang, S. Wang, G. Liu, Y. Xiao, C. Zuo, W. Tang, X. Fu, S. Dong, *J. Alloys Compd.* **2021**, *884*, 161147.

[50] T. Mageto, S. Bhoyate, K. Mensah-Darkw, A. Kumar, R. Gupt, *J. Energy Storage* **2023**, *70*, 108081.

[51] H. Alfaruqi, V. Mathew, J. Song, S. Kim, S. Islam, D. Pham, J. Jo, S. Kim, J. Baboo, Z. Xiu, K. Lee, Y. Sun, J. Kim, *Chem. Mater.* **2017**, *29*, 1684–1694.

[52] H. Cheng, Y. Zhang, X. Cai, C. Liu, Z. Wang, H. Ye, Y. Pan, D. Jia, H. Lin, *Small* **2023**, *20(5)*, 2305762.

[53] L. Xing, C. Zhang, M. Li, P. Hu, X. Zhang, Y. Dai, X. Pan, W. Sun, S. Li, J. Xue, Q. An, L. Mai, *Energy Storage Mater.* **2022**, *52*, 291–298.

[54] B. Lan, C. Tang, L. Chen, W. Zhang, W. Tang, C. Zuo, X. Fu, S. Dong, Q. An, P. Luo, *J. Alloys Compd.* **2020**, *818*, 153372.

[55] C. Mu, J. Mao, J. Guo, Q. Guo, Z. Li, W. Qin, Z. Hu, K. Davey, T. Ling, S. Qiao, *Adv. Mater.* **2020**, *32*, 1907168.

[56] Y. Xiao, J. Xiao, H. Zhao, J. Li, G. Zhang, D. Zhang, X. Guo, H. Gao, Y. Wang, J. Chen, G. Wang, H. Liu, *Small* **2024**, *20(35)*, 2401957.

[57] Z. Liu, P. Bertram, F. Endres, *J. Solid State Electrochem.* **2017**, *21*, 2021–2027.

[58] M. Li, M. Maisuradze, R. Sciacca, I. Hasa, M. Giorgetti, *Batteries & Supercaps* **2023**, *6*, e202300340.

[59] Y. Zeng, X. Lu, S. Zhang, D. Luan, S. Li, X. Lou, *Angew. Chem. Int. Ed.* **2021**, *60*, 22189–22194.

[60] J. Cao, Y. Xue, Z. Ji, J. Pu, X. Shen, L. Kong, A. Yuan, *J. Energy Storage* **2024**, *86*, 111413.

[61] Z. Jia, B. Wang, Y. Wang, *Mater. Chem. Phys.* **2015**, *149–150*, 601e606.

[62] R. Gupta, K. Ramanujam, *J. Chem. Sci.* **2024**, *136*, 19.

[63] J. Liu, Y. Zhou, G. Xing, M. Qi, Z. Tang, O. Terasaki, L. Chen, *Adv. Funct. Mater.* **2024**, *34*, 2312636.

[64] C. Hu, X. Yang, P. Liu, Z. Song, Y. Lv, L. Miao, M. Liu, L. Gan, *J. Mater. Chem. A* **2024**, *12*, 11867.

[65] S. Menart, K. Pirnat, D. Pahovnik, R. Dominko, *J. Mater. Chem. A* **2023**, *11*, 10874.

[66] O. Buyukcakir, R. Yuksel, F. Begar, M. Erdogmus, M. Arsakay, S. Lee, S. Kim, R. Ruof, *ACS Appl. Energ. Mater.* **2023**, *6*, 7672–7680.

[67] K. Pan, Y. Xie, Q. Hu, X. Zhang, S. Lu, Q. Li, H. Ji, *Mater. Lett.* **2022**, *311*, 131588.

[68] X. Yue, H. Liu, P. Liu, *Chem. Commun.* **2019**, *55*, 1647.

[69] G. Ren, Z. Luo, Y. Duan, X. Liu, Z. Yuan, F. Cai, *J. Alloys Compd.* **2022**, *898*, 162747.

[70] Z. Song, L. Miao, L. Ruhlmann, Y. Lv, L. Li, L. Gan, M. Liu, *Angew. Chem. Int. Ed.* **2023**, *62*, e202219136.

[71] Z. Song, L. Miao, H. Duan, Y. Lv, L. Gan, M. Liu, *Angew. Chem. Int. Ed.* **2024**, *63*, e202316835.

[72] X. Zheng, Z. Song, D. Zhang, W. Du, L. Miao, Y. Lv, L. Xie, L. Gan, M. Liu, *J. Mater. Chem. A* **2024**, *12*, 15352–15360.

[73] L. Zhang, S. Yang, W. Fu, Y. Cui, J. Wang, D. Zhao, C. Yang, X. Wang, B. Cao, *J. Mater. Sci. Technol.* **2022**, *127*, 206–213.

[74] W. Du, L. Miao, Z. Song, X. Zheng, Y. Lv, D. Zhu, L. Gan, M. Liu, *J. Power Sources* **2022**, *536*, 231512.

[75] D. Wang, L. Wang, G. Liang, H. Li, Z. Liu, Z. Tang, J. Liang, C. Zhi, *ACS Nano.* **2019**, *13*, 10643–10652.

[76] Y. Zhang, Z. Song, L. Miao, Y. Lv, L. Gan, M. Liu, *Adv. Funct. Mater.* **2024**, *34*, 2405710.

[77] Z. Yao, Q. Wu, K. Chen, J. Liu, C. Li, *Energy Environ. Sci.* **2020**, *13*, 3149.

[78] B. Sang, X. Wang, K. Feng, S. Gu, G. Li, K. Yue, Y. He, Q. Wang, T. Gao, G. Zhou, *J. Colloid Interface Sci.* **2024**, *653*, 199–208.

[79] Z. Luo, Z. Liu, H. He, Z. Zhang, Y. Chen, C. Peng, J. Zeng, *J. Mater. Sci. Technol.* **2023**, *145*, 93–100.

[80] K. Ran, Q. Chen, F. Song, F. Yang, *J. Colloid Interface Sci.* **2024**, *653*, 673–686.

[81] X. Liu, G. Xu, Q. Zhang, S. Huang, L. Li, X. Wei, J. Cao, L. Yang, P. Chu, *J. Power Sources* **2020**, *463*, 228223.

[82] H. Chen, W. Ma, J. Guo, J. Xiong, F. Hou, W. Si, Z. Sang, D. Yang, *J. Alloys Compd.* **2023**, *932*, 167688.

[83] L. Wang, X. Wang, B. Song, Z. Wang, L. Zhang, Q. Lu, *Surf. Interfaces.* **2022**, *33*, 102222.

[84] X. Liao, C. Pan, Y. Pan, C. Yin, *J. Alloys Compd.* **2021**, *888*, 161619.

[85] X. Cao, Y. Xu, B. Yang, H. Lang, Z. Shen, N. Wang, X. Wang, S. Wang, C. Sun, *J. Alloys Compd.* **2022**, *896*, 162785.

[86] T. Niu, J. Li, Y. Qi, X. Huang, Y. Ren, *J. Mater. Sci.* **2021**, *56*, 16582–16590.

[87] K. Cai, S. Luo, L. Qian, X. Meng, S. Yan, J. Guo, Q. Wang, X. Ji, X. Zhou, *J. Power Sources* **2023**, *564*, 232854.

[88] L. Jiang, F. Ye, Z. Wu, L. Zhang, Q. Liu, Z. Tang, L. Hu, *J. Mater. Chem. A* **2021**, *9*, 27380.

[89] Z. Fang, C. Liu, X. Li, L. Peng, W. Ding, X. Guo, W. Hou, *Adv. Funct. Mater.* **2023**, *33*, 2210010.

[90] D. Bin, W. Huo, Y. Yuan, J. Huang, Y. Liu, Y. Zhang, F. Dong, Y. Wang, Y. Xia, *Chem* **2020**, *6*, 968–984.

[91] F. Zhang, M. Du, Z. Miao, H. Li, W. Dong, Y. Sang, H. Jiang, W. Li, H. Liu, S. Wang, *InfoMat.* **2022**, *4*, e12346.

[92] X. Dan, X. Yin, J. Ba, J. Li, Y. Cheng, F. Duan, Y. Wei, Y. Wang, *Nano Lett.* **2024**, *24*, 6881–6888.

[93] X. Ma, X. Cao, M. Yao, L. Shan, X. Shi, G. Fang, A. Pan, B. Lu, J. Zhou, S. Liang, *Adv. Mater.* **2022**, *34*, 2105452.

[94] Y. Li, Y. Zhao, N. Wen, H. Zhou, Q. Kuang, Q. Fan, Y. Dong, *ACS Sustainable Chem. Eng.* **2023**, *11*, 5105–5114.

[95] Y. Tong, Y. Zang, S. Su, Y. Zhang, J. Fang, Y. Yang, X. Li, X. Wu, F. Chen, J. Hou, M. Luo, *J. Energy Chem.* **2023**, *77*, 269–279.

[96] K. James, S. Tang, W. Guo, Y. Fu, *ACS Appl. Mater. Interfaces* **2021**, *13*, 4084–4092.

[97] H. Zhang, D. Xu, L. Wang, Z. Ye, B. Chen, L. Pei, Z. Wang, Z. Cao, J. Shen, M. Ye, *Small* **2021**, *17*, 2100902.

[98] J. Wang, Z. Liu, H. Wang, F. Cui, G. Zhu, *Chem. Eng. J.* **2022**, *450*, 138051.

[99] X. Geng, Y. Jiang, H. Ma, H. Zhang, J. Liu, Z. Zhang, C. Peng, J. Zhang, Q. Zhao, N. Zhu, *ACS Appl. Mater. Interfaces* **2022**, *14*, 49746–49754.

[100] W. Du, J. Xiao, H. Geng, Y. Yang, Y. Zhang, E. Ang, M. Ye, C. Li, *J. Power Sources* **2020**, *450*, 227716.

[101] Q. Han, Y. Li, L. Han, Z. Lu, L. Liu, *Synth. Met.* **2024**, *301*, 117510.

[102] Z. Song, L. Miao, H. Duan, L. Ruhlman, Y. Lv, D. Zhu, L. Li, L. Gan, M. Liu, *Angew. Chem. Int. Ed.* **2022**, *61*, e202208821.

[103] M. Kamenskii, F. Volkov, S. Eliseeva, R. Holze, V. Kondratiev, *J. Electrochem. Soc.* **2023**, *170*, 010505.

[104] X. Liao, C. Pan, H. Yan, Y. Zhu, Y. Pan, C. Yin, *Chem. Eng. J.* **2022**, *440*, 135930.

[105] S. Zhang, W. Zhao, H. Li, Q. Xu, *ChemSusChem* **2020**, *13*, 188–195.

[106] Y. Liu, Z. Li, C. Li, Y. Wei, S. Yan, Z. Ji, S. Zou, H. Li, Y. Liu, C. Chen, X. He, M. Wu, *Chem. Eng. J.* **2024**, *488*, 150778.

[107] Y. Zhao, Y. Huang, F. Wu, R. Chen, L. Li, *Adv. Mater.* **2021**, *33*, 2106469.

[108] X. Cao, A. Xiao, Y. Hou, G. Liang, Y. Zhou, Y. Shi, C. Yue, Y. Zhu, Z. Zhao, J. Cuan, W. Li, *Int. J. Electrochem. Sci.* **2024**, *19*, 100583.

[109] Y. Zhao, Y. Huang, R. Chen, F. Wu, L. Li, *Mater. Horiz.* **2021**, *8*, 3124–3132.

[110] Z. Xu, L. Ruhlmann, Y. Lv, L. Gan, M. Liu, *ChemNanoMat* **2024**, *10*, e202300615.

[111] D. Selvakumaran, A. Pan, S. Liang, G. Cao, *J. Mater. Chem. A* **2019**, *7*, 18209–18236.

[112] T. Le, N. Sadique, L. Housel, A. Poyraz, E. Takeuchi, K. Takeuchi, A. Marschilok, P. Liu, *ACS Appl. Mater. Interfaces.* **2021**, *13*, 59937–59949.

[113] C. Xu, B. Li, H. Du, F. Kang, *Angew. Chem. Int. Ed.* **2012**, *51*, 933–935.

[114] M. Alfaruqi, J. Gim, S. Kim, J. Song, J. Jo, S. Kim, V. Mathew, J. Kim, *J. Power Sources.* **2015**, *288*, 320–327.

[115] M. Han, J. Huang, S. Liang, L. Shan, X. Xie, Z. Yi, Y. Wang, S. Guo, J. Zhou, *iScience* **2020**, *23*, 100797.

[116] W. Liu, X. Zhang, Y. Huang, B. Jiang, Z. Chang, C. Xu, F. Kang, *J. Energy Chem.* **2021**, *56*, 365–373.

[117] L. Wang, J. Zheng, *Mater. Today* **2020**, *7*, 100078.

[118] M. Zhang, R. Liang, T. Or, Y. Deng, A. Yu, Z. Chen, *Small Structures* **2021**, *2*, 2000064.

[119] X. Wu, C. Yin, M. Zhang, Y. Xie, J. Hu, R. Long, X. Wu, X. Wu, *Chem. Eng. J.* **2023**, *452*, 139573.

[120] Q. Sun, L. Chang, Y. Liu, W. Nie, T. Duan, Q. Xu, H. Cheng, X. Lu, *ACS Appl. Energ. Mater.* **2023**, *6*, 3102–3112.

[121] L. Hu, Q. Sun, H. Cai, J. Ni, J. Zhang, *Mater. Sci. Semicond. Process.* **2024**, *177*, 108358.

[122] X. Liang, Y. Yang, W. Di, S. Chen, R. Zhang, J. Hu, D. Lin, Y. Huo, *Chem. Eng. J.* **2024**, *495*, 153255.

[123] C. Hu, Y. Chen, Z. Song, L. Miao, H. Duan, Y. Lv, L. Xie, M. Liu, L. Gan, *J. Mater. Chem. A* **2024**, *12*, 12818–12825.

[124] M. Ni, M. Qin, H. Chang, X. Shi, B. Pei, S. Liang, X. Cao, *ChemSusChem* **2024**, *17(19)*, e202400526.